Technical Report

TR-2013-007

Variational Estimation of Cardiac Conductivities by a Data Assimilation Procedure

by

Huanhuan Yang, Alessandro Veneziani

Mathematics and Computer Science

EMORY UNIVERSITY

VARIATIONAL ESTIMATION OF CARDIAC CONDUCTIVITIES BY A DATA ASSIMILATION PROCEDURE

HUANHUAN YANG, ALESSANDRO VENEZIANI*

Abstract. Numerical simulations of cardiac potential are in general significantly sensitive to the parameters of the Bidomain model, the current standard model in electrocardiology. Unfortunately, these parameters - and in particular the cardiac conductivities - are quite problematic to measure *in vivo* and even more in clinical practice. On the other hand, no common agreement has been reached in the literature about cardiac conductivities. In this paper, we consider a data assimilation approach for estimating those parameters. More specifically, we consider the parameters as control variables to minimize the mismatch between the computed and the measured potentials, under the constraint of the Bidomain equations. The functional to be minimized is suitably regularized a lá Tikhonov. We prove the existence of a minimizer and we solve the problem with the BFGS method based on dual equations, showing that this method compares favorably with other methods present in the literature. We provide preliminary numerical results in 2D, showing the reliability of the approach with different numbers of measurement sites and in presence of noise.

Key words. cardiac conductivity, bidomain model, variational data assimilation

1. Introduction. Numerical methods have been used for investigating cardiovascular diseases since at least 25 years. Moving from idealized and simplified models, computational tools have been progressively refined and applied to patient specific geometries retrieved from medical images. An extensive use of numerical investigations in the clinical practice is however prevented for several reasons. One is the uncertainty affecting the numerical models when applied to a specific patient. In practice, mathematical models depend on parameters that typically come from appropriate constitutive laws and the precise quantification of these parameters for a patient may be problematic. For this reason, methods of *data assimilation* have been advocated recently in cardiovascular mathematics . By this we mean numerical techniques for merging available patient specific measures (that we call our *foreground or patient specific knowledge*) with mathematical numerical models (the *background or general knowledge*) with the twofold aim of filtering the noise in the data and reducing uncertainty in the model by a precise quantification of parameters (see e.g. [6, 32]). This paper aims at a variational patient-specific estimation of cardiac conductivities based on available measures of cardiac potential.

Computational electrocardiology is a well established field, whose importance relies upon both the intrinsic challenging mathematical and numerical features and the practical relevance to cardiac physiopathology [4, 14, 25, 28]. Although the significance of a precise patient specific conductivity estimation has been recognized since a long time [29] and experimental methods based on controlled measurements after an appropriate stimulus of the tissue are quite impractical in clinics, computational methods have been advocated only in the last few years. After the work of Geselowitz [7], experimental estimation of the intracellular and extracellular conductivities has been carried out in different ways by several groups [5, 26, 27], leading to different ranges of possible values with no common agreement on the most accurate ones. These values are reported in Table 1.1. Here σ_{il} (σ_{it}) denotes the longitudinal (tangential) intracellular conductivity, while σ_{el} (σ_{et}) is the extracellular counterpart. It is worth stressing that the Bidomain equations - one of the most popular mathematical mod-

*Department of Mathematics and Computer Science, Emory University, Atlanta (GA) USA, avenez2@emory.edu, huanhuan.yang@emory.edu

TABLE 1.1
Values of bidomain conductivities proposed in [9] (mS/cm).

Param ↓ \ Ref →	Clerc [5]	Roberts et al.[26]	Roberts and Scher[27]
σ_{il}	1.70	2.80	3.40
σ_{it}	0.19	0.26	0.60
σ_{el}	6.20	2.20	1.20
σ_{et}	2.40	1.30	0.80
σ_{il}/σ_{it}	8.95	10.77	5.67
σ_{el}/σ_{et}	2.58	1.69	1.50
σ_{il}/σ_{el}	0.27	1.27	2.83
σ_{it}/σ_{et}	0.08	0.20	0.75

els in computational electrocardiology - have been proved to be strongly sensitive to the values of conductivities and in particular to the ratio between the tangential and longitudinal extracellular conductivities [13].

Computational models based on multiscale arguments, where tissue-scale parameters are estimated by the simulation of cell-scale models, have been explored in [30, 31]. The so-called *4-leads method* requires the virtual placement of leads at a distance of the order of microns [18, 29] and a variational procedure for extracting the conductivities from a series of controlled current stimuli of the cardiac tissue. More recently, a variational approach for a reliable estimation of conductivities has been proposed in [9, 10]. This method is based on a classical least square procedure. Results presented in [9] refer to 2D synthetic cases and clearly show that the variational estimate may provide accurate results, but it is computationally expensive (at least 80 solutions of the 2D Bidomain system are required) and results are sensitive to the noise. Moreover, addition of more parameters to be estimated (like the fiber orientation) may in fact prevent the convergence of the iterative method.

In this paper we still refer to a variational procedure for the estimation of cardiac conductivities from measures of the transmembrane potential available in some sites on the tissue. We provide a rigorous mathematical formulation of the problem based on constrained minimization arguments and a well-posedness analysis. Contrarily to the least-square approach of [9], our numerical procedure is based on the classical Lagrange multiplier approach. Constrained minimization is performed by a gradient-descent method. The gradient of the functional to be minimized is solved by resorting to the dual equations of the Bidomain system. In particular, we pursue an Optimize-then-Discretize approach, leading to the solution of a backward in time set of equations. In this first paper, results are presented in a 2D synthetic setting.

We present the inverse conductivity problem (ICP) in Section 2. The formulation and the equations to be solved in the variational approach are presented. Well posedness analysis, inspired by the work of Kunisch and co-workers for the optimization of the pace-making stimulus [16, 17, 15], is carried out in Section 3. Numerical solver is explained in detail in Section 4. Finally, in Section 5 we illustrate several numerical tests with data generated by accurate numerical procedures and added by noise. Results lead to the conclusion that the approach presented here do improve the least-square method in terms of efficiency and provide a reliable and potentially practical method for estimating the cardiac conductivities (Section 6).

Follow-up of this work is the extension of the procedure to 3D geometries and

experimental validation of the method in view of clinical applications. A reliable estimation of patient-specific conductivities is actually essential for an extensive use of computational models in clinics.

2. The Inverse Conductivity Problem.

2.1. The Bidomain model (Forward Problem). Let $\Omega \subset \mathbb{R}^d (d = 2 \text{ or } 3)$ be a bounded domain, and $[0, T]$ a fixed time interval. The bidomain model is derived from the current conservation

$$\begin{cases} \nabla \cdot \bar{\boldsymbol{\sigma}}_i \nabla \phi_i = \beta(I_m - \bar{I}_{si}), \quad \nabla \cdot \bar{\boldsymbol{\sigma}}_e \nabla \phi_e = -\beta(I_m - \bar{I}_{se}) \\ \text{with} \quad I_m = C_m \dfrac{\partial V_m}{\partial t} + I_{ion} \end{cases} \tag{2.1}$$

where ϕ_i, ϕ_e denote the intracellular and extracellular electric potentials,$V_m = \phi_i - \phi_e$ is the transmembrane potential, $\bar{\boldsymbol{\sigma}}_i, \bar{\boldsymbol{\sigma}}_e$ are the conductivity tensors, β is the ratio of membrane area per tissue volume, I_m is the ingoing membrane current flow with C_m being the capacitance and I_{ion} the ionic current. $\bar{I}_{si}, \bar{I}_{se}$ represent the intracellular and extracellular stimulation currents respectively.

Let $Q = \Omega \times [0, T]$, and $\partial Q = \partial\Omega \times [0, T]$. We set $u = V_m, u_e = \phi_e$, then the complete bidomain model in a parabolic-elliptic form (see e.g. [25]) is

$$\begin{cases} \dfrac{\partial u}{\partial t} - \nabla \cdot \boldsymbol{\sigma}_i \nabla u - \nabla \cdot \boldsymbol{\sigma}_i \nabla u_e + f(u, w) = I_{si} & \text{in } Q \\ -\nabla \cdot \boldsymbol{\sigma}_i \nabla u - \nabla \cdot (\boldsymbol{\sigma}_i + \boldsymbol{\sigma}_e) \nabla u_e = I_{si} - I_{se} & \text{in } Q \\ \dfrac{\partial w}{\partial t} + g(u, w) = 0 & \text{in } Q \\ (\boldsymbol{\sigma}_i \nabla u + \boldsymbol{\sigma}_i \nabla u_e) \cdot \mathbf{n} = 0, \quad \boldsymbol{\sigma}_e \nabla u_e \cdot \mathbf{n} = 0 & \text{on } \partial Q \\ u(x, 0) = u_0, \quad w(x, 0) = w_0 & \text{in } \Omega \end{cases} \tag{2.2}$$

where

$$I_{si,se} = \frac{1}{C_m} \bar{I}_{si,se}, \quad f(u, w) = \frac{1}{C_m} I_{ion}(u, w),$$

$$\boldsymbol{\sigma}_i = \frac{1}{\beta C_m} \bar{\boldsymbol{\sigma}}_i = \frac{1}{\beta C_m} (\sigma_{il} \mathbf{a_l} \mathbf{a_l}^t + \sigma_{it} \mathbf{a_t} \mathbf{a_t}^t + \sigma_{in} \mathbf{a_n} \mathbf{a_n}^t),$$

$$\boldsymbol{\sigma}_e = \frac{1}{\beta C_m} \bar{\boldsymbol{\sigma}}_e = \frac{1}{\beta C_m} (\sigma_{el} \mathbf{a_l} \mathbf{a_l}^t + \sigma_{et} \mathbf{a_t} \mathbf{a_t}^t + \sigma_{en} \mathbf{a_n} \mathbf{a_n}^t),$$

$(\mathbf{a_l}, \mathbf{a_t}, \mathbf{a_n})$ are orthonormal vectors related to the structure of the myocardium with $\mathbf{a_l}$ parallel to the local fibre direction. f and g are functions associated with the ionic activity, and w is the recovery variable in the ionic model.

2.2. Variational formulation of the inverse problem. Let the admissible domain for control variables be $\mathcal{C}_{ad}^{3D}$ (or $\mathcal{C}_{ad}^{2D}$):

$$\mathcal{C}_{ad}^{3D} = \{\boldsymbol{\sigma} = (\sigma_{il}, \sigma_{it}, \sigma_{in}, \sigma_{el}, \sigma_{et}, \sigma_{en}) \in (L^\infty(\Omega))^6 : \boldsymbol{\sigma}(x) \in [m, M]^6, \forall x \in \Omega\},$$

$$\mathcal{C}_{ad}^{2D} = \{\boldsymbol{\sigma} = (\sigma_{il}, \sigma_{it}, \sigma_{el}, \sigma_{et}) \in (L^\infty(\Omega))^4 : \boldsymbol{\sigma}(x) \in [m, M]^4, \forall x \in \Omega\},$$

where m and M are positive constants. The problem we want to investigate, which we call *inverse conductivity problem* (ICP), reads: find $\boldsymbol{\sigma} \in \mathcal{C}_{ad}^{3D}$ (or $\mathcal{C}_{ad}^{2D}$) that minimizes the functional

$$\mathcal{J}(\boldsymbol{\sigma}) = \frac{1}{2}\int_0^T \int_{\Omega_{obs}} (u - u_{meas})^2 \; dxdt + \frac{\alpha}{2}\int_\Omega ||\boldsymbol{\sigma} - \hat{\boldsymbol{\sigma}}||^2 dx \tag{2.3}$$

subject to the bidomain equations (2.2). Here u_{meas} denotes the experimental data, which is measued on the observation domain $\Omega_{obs} \subset \Omega$, $\hat{\boldsymbol{\sigma}}$ is the mean of conductivity values from literatures, and $\|\cdot\|$ denotes the Euclidean norm. Here α is the Tikhonov regularization coefficient, used to weigh the relevance of the regularization in the minimization procedure.

We introduce the Lagrangian functional

$$\begin{aligned}
&\mathcal{L}(u, u_e, w, \boldsymbol{\sigma}, p, q, r) = \mathcal{J}(u, \boldsymbol{\sigma}) \\
&+ \textstyle\int_0^T \int_\Omega (\nabla \cdot (\boldsymbol{\sigma}_i + \boldsymbol{\sigma}_e)\nabla u_e + \nabla \cdot \boldsymbol{\sigma}_i \nabla u + I_{si} - I_{se}) p \; dxdt \\
&+ \textstyle\int_0^T \int_\Omega (-\frac{\partial u}{\partial t} + \nabla \cdot \boldsymbol{\sigma}_i \nabla u + \nabla \cdot \boldsymbol{\sigma}_i \nabla u_e - f(u, w) + I_{si}) q \; dxdt \\
&+ \textstyle\int_0^T \int_\Omega (-\frac{\partial w}{\partial t} - g(u, w)) r \; dxdt
\end{aligned} \tag{2.4}$$

where $p,\ q,$ and r are the Lagrange multipliers.

Setting the partial derivatives of $\mathcal{L}$ with respect to u_e equal to zero, we deduce

$$\begin{cases} \nabla \cdot (\boldsymbol{\sigma}_i + \boldsymbol{\sigma}_e)\nabla p + \nabla \cdot \boldsymbol{\sigma}_i \nabla q = 0 & \text{in } Q \\ (\boldsymbol{\sigma}_i + \boldsymbol{\sigma}_e)\nabla p \cdot \mathbf{n} + \boldsymbol{\sigma}_i \nabla q \cdot \mathbf{n} = 0 & \text{on } \partial Q \end{cases} \tag{2.5}$$

Correspondingly, setting the partial derivatives of $\mathcal{L}$ with respect to u equal to zero deduce

$$\begin{cases} \dfrac{\partial q}{\partial t} + \nabla \cdot \boldsymbol{\sigma}_i \nabla p + \nabla \cdot \boldsymbol{\sigma}_i \nabla q - f_{,u} q - g_{,u} r = -(u - u_{meas})\chi_{\Omega_{obs}} & \text{in } Q \\ \boldsymbol{\sigma}_i \nabla p \cdot \mathbf{n} + \boldsymbol{\sigma}_i \nabla q \cdot \mathrm{n} = 0 & \text{on } \partial Q \\ q(T) = 0 & \text{in } \Omega \end{cases} \tag{2.6}$$

where $f_{,u}$ means the derivative $\frac{\partial f}{\partial u}$, and so is the case for other similar notations. Setting the partial derivatives of $\mathcal{L}$ with respect to w equal to zero, we find

$$\begin{cases} \dfrac{\partial r}{\partial t} - g_{,w}\ r - f_{,w}\ q = 0 & \text{in } Q \\ r(T) = 0 & \text{in } \Omega \end{cases} \tag{2.7}$$

To summarize, we have constructed the *dual equations* (2.5)-(2.7) as a dual form of the Bidomain equations, which we call the *state equations*.

For the sake of simplicity, from now on we consider the 2D case. However, it is worth noting that the well posedness analysis that follows is promptly extended to the 3D case. In material coordinates, the conductivity tensors read $\boldsymbol{\sigma}_i^* = \begin{bmatrix} \sigma_{il} & 0 \\ 0 & \sigma_{it} \end{bmatrix}, \boldsymbol{\sigma}_e^* = \begin{bmatrix} \sigma_{el} & 0 \\ 0 & \sigma_{et} \end{bmatrix}$. Let A be the transformation from the global coordinates to the material coordinates, θ be the fibre angle, then A is given by $A = \begin{pmatrix} \cos\theta & \sin\theta \\ -\sin\theta & \cos\theta \end{pmatrix}$. Therefore we have the conductivity tensors in the global coordinates $\boldsymbol{\sigma}_i = A^t \boldsymbol{\sigma}_i^* A, \boldsymbol{\sigma}_e = A^t \boldsymbol{\sigma}_e^* A$.

Following [11], we compute the gradient of $\mathcal{J}$ with respect to the control variables, i.e. the conductivities, by resorting to the dual equations and the formulation of sensitivity equations. By direct(formal) differentiation with respect to the control variable σ_{il}, we get

$$\frac{\mathcal{D}\mathcal{J}}{\mathcal{D}\sigma_{il}} = \int_0^T \int_\Omega (u - u_{meas}) \chi_{\Omega_{obs}} \frac{\partial u}{\partial \sigma_{il}} \, dxdt + \alpha \int_\Omega (\sigma_{il} - \hat{\sigma}_{il}) \, dx. \tag{2.8}$$

Here the sensitivity $\frac{\partial u}{\partial \sigma_{il}}$ can be determined by the equations derived from direct differentiation of the state equations with respect to σ_{il}. For instance, differentiation of the second equation in (2.2) with respect to σ_{il} deduces

$$-\nabla \cdot \boldsymbol{\sigma}_i \nabla \frac{\partial u}{\partial \sigma_{il}} - \nabla \cdot \Theta_l \nabla u - \nabla \cdot (\boldsymbol{\sigma}_i + \boldsymbol{\sigma}_e) \nabla \frac{\partial u_e}{\partial \sigma_{il}} - \nabla \cdot \Theta_l \nabla u_e = 0,$$

where $\Theta_l = \dfrac{1}{\beta C_m} \begin{pmatrix} \cos^2\theta & \sin\theta\cos\theta \\ \sin\theta\cos\theta & \sin^2\theta \end{pmatrix}$.

Suppose (p, q, r) is the solution of the dual equations, we use the first equation in (2.6) to substitute for $(u - u_{meas})\chi_{\Omega_{obs}}$ in (2.8). After simplification using the sensitivity equations and the Green's identity, we get

$$\frac{\mathcal{D}\mathcal{J}}{\mathcal{D}\sigma_{il}} = -\int_0^T \int_\Omega \Theta_l \nabla(u + u_e) \cdot \nabla(p + q) \, dxdt + \alpha \int_\Omega (\sigma_{il} - \hat{\sigma}_{il}) \, dx. \tag{2.9}$$

Similarly, we can also get

$$\frac{\mathcal{D}\mathcal{J}}{\mathcal{D}\sigma_{it}} = -\int_0^T \int_\Omega \Theta_t \nabla(u + u_e) \cdot \nabla(p + q) \, dxdt + \alpha \int_\Omega (\sigma_{it} - \hat{\sigma}_{it}) \, dx \tag{2.10}$$

$$\frac{\mathcal{D}\mathcal{J}}{\mathcal{D}\sigma_{el}} = -\int_0^T \int_\Omega \Theta_l \nabla u_e \cdot \nabla p \, dxdt + \alpha \int_\Omega (\sigma_{el} - \hat{\sigma}_{el}) \, dx \tag{2.11}$$

$$\frac{\mathcal{D}\mathcal{J}}{\mathcal{D}\sigma_{et}} = -\int_0^T \int_\Omega \Theta_t \nabla u_e \cdot \nabla p \, dxdt + \alpha \int_\Omega (\sigma_{et} - \hat{\sigma}_{et}) \, dx \tag{2.12}$$

where $\Theta_t = \dfrac{1}{\beta C_m} \begin{pmatrix} \sin^2\theta & -\sin\theta\cos\theta \\ -\sin\theta\cos\theta & \cos^2\theta \end{pmatrix}$.

3. Well posedness analysis. In this section we prove the existence of a minimizer. The proof is inspired by Kunisch et al.[22] for the optimization problem about pacemaker stimuli.

We denote $V = H^1(\Omega), H = L^2(\Omega), U = V/\mathbb{R} = \{[u] = u - \frac{1}{|\Omega|}\int_\Omega u : u \in H^1(\Omega)\}$. The quotient space is used because the solution u_e is determined up to an additive constant. To simplify the notation, we use $L^2(V)$ instead of $L^2(0,T;V)$. V^* denotes the dual space of V. $\mathcal{D}(0,T)$ is the space of C^∞ functions on $\mathbb{R}$ with compact support in $(0,T)$. The space of all distributions on $\mathcal{D}(0,T)$ is denoted by $\mathcal{D}'(0,T)$.

We postulate the following assumptions on the data:

1. Ω is a bounded domain in $\mathbb{R}^d (d = 2 \text{ or } 3)$ with Lipschitz boundary $\partial\Omega$.
2. The conductivity tensors $\boldsymbol{\sigma}_i$ and $\boldsymbol{\sigma}_e$ are uniformly elliptic. Namely, there exist constants $m,\ M > 0$ such that

$$\forall \xi \in \mathbb{R}^d,\ m|\xi|^2 \le \xi^t \boldsymbol{\sigma}_{i,e}(x)\xi \le M|\xi|^2, \text{ for all } x \in \Omega.$$

3. I_{si} and I_{se} belong to $L^2(0,T;V^*)$, and satisfy the compatibility condition $\int_\Omega (I_{si} - I_{se})dx = 0$ for a.e. $t \in [0,T]$.
4. The initial data u_0, w_0 belong to the space $L^2(\Omega)$.
5. We assume in particular to work with the Rogers-McCulloch ionic model. In a simplified setting[1], in particular, f and g are given as:

$$f(u,w) = bu(u-a)(u-1) + uw, \quad g(u,w) = \epsilon(-ku + w) \tag{3.1}$$

with $0 < a < 1, b, k, \epsilon > 0$.

Definition 3.1 (Weak Solution). *$(u, u_e, w) \in (L^2(V) \cap L^4(Q) \cap C(H)) \times L^2(U) \times C(H)$ is called a weak solution of system (2.2), if $u(0) = u_0, w(0) = w_0$, and (u, u_e, w) verify in $\mathcal{D}'(0,T)$:*

$$\frac{d}{dt}\int_\Omega u(t)\varphi + \int_\Omega \boldsymbol{\sigma}_i \nabla(u(t) + u_e(t)) \cdot \nabla\varphi + \int_\Omega f(u(t), w(t))\varphi = \int_\Omega I_{si}(t)\varphi, \quad \forall \varphi \in V \tag{3.2}$$

$$\int_\Omega \boldsymbol{\sigma}_i \nabla u(t) \cdot \nabla\phi + \int_\Omega (\boldsymbol{\sigma}_i + \boldsymbol{\sigma}_e)\nabla u_e(t) \cdot \nabla\phi = \int_\Omega (I_{si}(t) - I_{se}(t))\phi, \quad \forall \phi \in U \tag{3.3}$$

$$\frac{d}{dt}\int_\Omega w(t)\psi + \int_\Omega g(u(t), w(t))\psi = 0, \quad \forall \psi \in H \tag{3.4}$$

We define $a_{i,e} : V \times V \to \mathbb{R}$ or $U \times U \to \mathbb{R}$ by

$$a_i(u,v) = \int_\Omega \boldsymbol{\sigma}_i \nabla u \cdot \nabla v dx, \quad a_e(u,v) = \int_\Omega \boldsymbol{\sigma}_e \nabla u \cdot \nabla v dx.$$

Theorem 3.2 ([3] Theorem 30). *Under the five assumptions specified before, the bidomain system (2.2) has a weak solution (u, u_e, w).*

Lemma 3.3 (A priori estimates, [22] Lemma 3.5). *With the assumption in theorem 3.2, there exist positive constants $\tilde{C}$ and $\tilde{c}$, such that*

$$|u|_{C(H)} + |u|_{L^2(V)} + |u|_{L^4(Q)} + |u_t|_{L^{4/3}(V^*)} + |v|_{L^2(U)} + |w|_{C(H)} + |w_t|_{L^2(H)}$$

[1] In Section 5 we will use a slightly different formulation of the ionic model. However, it is equivalent to the one we use here for the sake of simplicity when we do the well posedness analysis.

$$\leq \tilde{C}(|u_0| + |v_0| + \tilde{c}|\Omega| + |I_{si}|_{L^2(V^*)} + |I_{si} - I_{se}|_{L^2(U^*)}). \tag{3.5}$$

where $\tilde{c}$ depends on the ionic model, $\tilde{C}$ depends on m, M and the ionic model, but is independent of $(u_0, w_0), (I_{si}, I_{se})$ and $\boldsymbol{\sigma}_{i,e}$.

THEOREM 3.4 (Existence of minimizer). *Under the assumption condition as before, for $\alpha \geq 0$, there exists at least one minimizer to the optimization problem.*

Proof. Recall that the admissible domain for control variables is[2] $\mathcal{C}_{ad} = \mathcal{C}_{ad}^{2D} = \{\boldsymbol{\sigma} = (\sigma_{il}, \sigma_{it}, \sigma_{el}, \sigma_{et}) \in (L^\infty(\Omega))^4 : \boldsymbol{\sigma}(x) \in [m, M]^4, \forall x \in \Omega\}$. Since $\mathcal{J}$ is bounded from below, $\inf_{\boldsymbol{\sigma} \in \mathcal{C}_{ad}} \mathcal{J}(\boldsymbol{\sigma}) \in \mathbb{R}$ and there exists a minimizing sequence $\boldsymbol{\sigma}^{(k)} \in \mathcal{C}_{ad}$, such that

$$\lim_{k \to \infty} \mathcal{J}(\boldsymbol{\sigma}^{(k)}) = \inf_{\boldsymbol{\sigma} \in \mathcal{C}_{ad}} \mathcal{J}(\boldsymbol{\sigma}).$$

Because $\{\boldsymbol{\sigma}^{(k)}\}$ are bounded in $(L^\infty(\Omega))^4$, it follows from the weak compactness property that there exists a subsequence of $\boldsymbol{\sigma}^{(k)}$, which we denote by the same symbol, such that

$$\boldsymbol{\sigma}^{(k)} \to \boldsymbol{\sigma}^* \quad \text{weakly-} * \text{ in } (L^\infty(\Omega))^4. \tag{3.6}$$

We claim that $\boldsymbol{\sigma}^* \in \mathcal{C}_{ad}$. Indeed, if for example $\Gamma = \{x : \sigma_{il}^*(x) > M\}$ have positive measure, then $\int_\Omega (\sigma_{il}^*(x) - \sigma_{il}^{(k)}) \chi_\Gamma dx \geq \int_\Gamma (\sigma_{il}^*(x) - M) dx > 0$, which leads to a contradiction, since for $k \to \infty$, the left hand side is zero. So is the case for the lower bound m.

Let $(u^{(k)}, u_e^{(k)}, w^{(k)})$ be the associated solutions with $\boldsymbol{\sigma}^{(k)}$, by the *a priori* estimate and weak compactness property, there exists a subsequence of $(u^{(k)}, u_e^{(k)}, w^{(k)}, \boldsymbol{\sigma}^{(k)}) \in (L^2(V) \cap L^4(Q)) \times L^2(U) \times C(H) \times (L^\infty(\Omega))^4$, denote by the same sequence, such that

$$u^{(k)} \rightharpoonup u \text{ in } L^2(V) \cap L^4(Q), \quad u_e^{(k)} \rightharpoonup u_e \text{ in } L^2(U), \quad w^{(k)} \rightharpoonup w \text{ in } L^2(H) \tag{3.7}$$

$$\frac{d}{dt} u^{(k)} \rightharpoonup \frac{d}{dt} u \text{ in } L^{4/3}(V^*), \quad \frac{d}{dt} w^{(k)} \rightharpoonup \frac{d}{dt} w \text{ in } L^2(H) \tag{3.8}$$

Let the corresponding bilinear forms associated with $\{\boldsymbol{\sigma}^{(k)}, \boldsymbol{\sigma}^*\}$ be $\{a_{i,e}^k, a_{i,e}^*\}$:

$$a_{i,e}^k(u, v) = \int_\Omega \boldsymbol{\sigma}_{i,e}^{(k)} \nabla u \cdot \nabla v, \quad a_{i,e}^*(u, v) = \int_\Omega \boldsymbol{\sigma}_{i,e}^* \nabla u \cdot \nabla v.$$

Since the conductivity tensors are uniformly elliptic, $|a_i^*(u, v)| \leq M ||u||_V ||v||_V$. This means for fixed $v \in V$, $a_i^* \in V^*$. Since $u^{(k)}$ is weakly convergent and $\phi v \in L^4(Q) \cap L^2(V)$ for any $\phi \in \mathcal{D}(0, T)$, we have

$$\int_0^T a_i^*(u^{(k)}, \phi v) dt \to \int_0^T a_i^*(u, \phi v) dt, \quad \forall\ \phi \in \mathcal{D}(0, T),\ v \in V. \tag{3.9}$$

[2]Should we use $\mathcal{C}_{ad} = \mathcal{C}_{ad}^{3D}$, the proof follows similar arguments in 3D.

For any fixed $\phi \in \mathcal{D}(0,T)$ and $\psi \in \mathcal{C}_0^\infty(\mathbb{R}^d)$, we have

$$\begin{aligned}
&\int_0^T a_i^k(u^{(k)}, \phi\psi)dt - \int_0^T a_i^*(u^{(k)}, \phi\psi)dt \\
=&(\int_0^T \int_\Omega (\sigma_{il}^{(k)} - \sigma_{il}^*)\mathbf{a_l}\mathbf{a_l}^t \nabla u^{(k)} \cdot \nabla(\phi\psi) + \int_0^T \int_\Omega (\sigma_{it}^{(k)} - \sigma_{it}^*)\mathbf{a_t}\mathbf{a_t}^t \nabla u^{(k)} \cdot \nabla(\phi\psi) \\
+&\int_0^T \int_\Omega (\sigma_{in}^{(k)} - \sigma_{in}^*)\mathbf{a_n}\mathbf{a_n}^t \nabla u^{(k)} \cdot \nabla(\phi\psi)) \cdot \frac{1}{\beta C_m} \\
=&(\int_0^T \int_\Omega (\sigma_{il}^{(k)} - \sigma_{il}^*)\mathbf{a_l}^t \nabla(\phi\psi)\mathbf{a_l}^t \nabla u^{(k)} + \int_0^T \int_\Omega (\sigma_{it}^{(k)} - \sigma_{it}^*)\mathbf{a_t}^t \nabla(\phi\psi)\mathbf{a_t}^t \nabla u^{(k)} \\
+&\int_0^T \int_\Omega (\sigma_{in}^{(k)} - \sigma_{in}^*)\mathbf{a_n}^t \nabla(\phi\psi)\mathbf{a_n}^t \nabla u^{(k)}) \cdot \frac{1}{\beta C_m}
\end{aligned}$$

Notice that $\mathbf{a_l}$ has unit length and $\nabla(\phi\psi)$ is in $L^\infty(Q;\mathbb{R}^d)$. While $\{\boldsymbol{\sigma}^{(k)}\}$ can be treated as weakly-$*$ convergent to $\boldsymbol{\sigma}^*$ in $(L^\infty(Q))^4$, We have $\{\boldsymbol{\sigma}^{(k)}\mathbf{a_l}^t \nabla(\phi\psi)\}$ weakly-$*$ convergent to $\boldsymbol{\sigma}^*\mathbf{a_l}^t \nabla(\phi\psi)$ in $(L^\infty(Q))^4$. From

$$||\nabla u^{(k)}||_{L^1(Q;\mathbb{R}^d)} \leq (|\Omega|T)^{1/2}||\nabla u^{(k)}||_{L^2(Q;\mathbb{R}^d)}$$

and the *a priori* estimate, we see $\{\nabla u^{(k)}\}$ is bounded in $L^1(Q;\mathbb{R}^d)$. So by passing to a subsequence, we can require $\nabla u^k \rightharpoonup \nabla u$ in $L^1(Q;\mathbb{R}^d)$. The Dunford-Pettis property of $L^1(Q)$ (see [19], section 1.6) thus leads to the following convergence

$$\int_0^T \int_\Omega (\sigma_{il}^{(k)} - \sigma_{il}^*)\mathbf{a_l}^t \nabla(\phi\psi)\mathbf{a_l}^t \nabla u^{(k)} \to 0, \text{ as } k \to \infty. \tag{3.10}$$

Doing in the same way for the other two terms we then have

$$\int_0^T a_i^k(u^{(k)}, \phi\psi)dt - \int_0^T a_i^*(u^{(k)}, \phi\psi)dt \to 0, \text{ as } k \to \infty \quad \forall\ \phi \in \mathcal{D}(0,T),\ \psi \in \mathcal{C}_0^\infty(\mathbb{R}^d).$$

Since Ω has Lipschitz boundary, it then satisfies the segment condition(see [1], definition 3.21). We say $\mathcal{C}_0^\infty(\mathbb{R}^d)$ is dense in V(see [1], theorem 3.22). Therefore we have

$$\int_0^T a_i^k(u^{(k)}, \phi v)dt - \int_0^T a_i^*(u^{(k)}, \phi v)dt \to 0, \text{ as } k \to \infty, \quad \forall\ \phi \in \mathcal{D}(0,T),\ v \in V.$$

Combined with limit (3.9) this convergence deduces

$$\int_0^T a_i^k(u^{(k)}, \phi v)dt - \int_0^T a_i^*(u, \phi v)dt \to 0, \text{ as } k \to \infty, \quad \forall\ \phi \in \mathcal{D}(0,T),\ v \in V. \tag{3.11}$$

Similarly, we can have

$$\int_0^T a_i^k(u_e^{(k)}, \phi v)dt - \int_0^T a_i^*(u_e, \phi v)dt \to 0, \text{ as } k \to \infty, \quad \forall\ \phi \in \mathcal{D}(0,T),\ v \in V. \tag{3.12}$$

$$\int_0^T a_e^k(u_e^{(k)}, \phi v)dt - \int_0^T a_e^*(u_e, \phi v)dt \to 0, \text{ as } k \to \infty, \quad \forall\ \phi \in \mathcal{D}(0,T),\ v \in V. \tag{3.13}$$

For the convergence of other terms in equations (3.2)-(3.4), we refer to the proof in [3] p.477. At the end, by passing to the limit in the equations satisfied by $(u^{(k)}, u_e^{(k)}, w^{(k)}, \boldsymbol{\sigma}^{(k)})$ we argue that $(u, u_e, w, \boldsymbol{\sigma}^*)$ is a solution to the bidomain equations.

We conclude then that $\boldsymbol{\sigma}^*$ realizes the minimum of $\mathcal{J}$. By the Rellich-Kondrachov embedding theorem, $u^{(k)}$ converge strongly to u in $L^2(Q)$. In fact, from convergence (3.6) it follows that $\{\boldsymbol{\sigma}^{(k)}\}$ is also weakly convergent in $(L^2(\Omega))^4$. The weak lower semicontinuity of $\int_\Omega ||\boldsymbol{\sigma}^{(k)} - \hat{\boldsymbol{\sigma}}||^2 dx$ in $L^2(\Omega)$ then implies that

$$\begin{aligned}
\mathcal{J}(\boldsymbol{\sigma}^*) &= \frac{1}{2}\int_0^T \int_\Omega (u - u_{meas})^2 dxdt + \frac{\alpha}{2}\int_\Omega ||\boldsymbol{\sigma}^* - \hat{\boldsymbol{\sigma}}||^2 dx \\
&\leq \frac{1}{2}\lim_{k\to\infty}\int_0^T \int_\Omega (u^{(k)} - u_{meas})^2 dxdt + \frac{\alpha}{2}\liminf_{k\to\infty}\int_\Omega ||\boldsymbol{\sigma}^{(k)} - \hat{\boldsymbol{\sigma}}||^2 dx \\
&\leq \liminf_{k\to\infty}(\frac{1}{2}\int_0^T \int_\Omega (u^{(k)} - u_{meas})^2 dxdt + \frac{\alpha}{2}\int_\Omega ||\boldsymbol{\sigma}^{(k)} - \hat{\boldsymbol{\sigma}}||^2 dx) \\
&= \lim_{k\to\infty}\mathcal{J}(\boldsymbol{\sigma}^{(k)}) = \inf_{\boldsymbol{\sigma}\in\mathcal{C}_{ad}}\mathcal{J}(\boldsymbol{\sigma}),
\end{aligned}$$

and the existence of minimizer is proved. □

Remark 1. When $\mathcal{J}$ has a minimum at $\boldsymbol{\sigma}^*$ belonging to the interior of $\mathcal{C}_{ad}$, the derivatives of J in any direction are zero, which leads to the KKT system. However, $\boldsymbol{\sigma}^*$ could be on the boundary $\partial\mathcal{C}_{ad}$. In this case, the solution is not a stationary point of the mismatch functional. Nevertheless, there are some special choices of the regularization term to make sure $\boldsymbol{\sigma}^*$ belongs to the interior of $\mathcal{C}_{ad}$. For example, we can choose $R_2 = \frac{\alpha}{2}\int_\Omega ||\log\boldsymbol{\sigma} - \log\hat{\boldsymbol{\sigma}}||^2 dx$ as the regularization term. In this case,

$$R_2 = \frac{\alpha}{2}\int_\Omega ||\log\boldsymbol{\sigma} - \log\hat{\boldsymbol{\sigma}}||^2 dx \to \infty, \text{ as } \boldsymbol{\sigma} \to 0 \text{ or } \boldsymbol{\sigma} \to \infty.$$

Notice that the first term in $\mathcal{J}$ is non-negative, so a proper choice of m and M guarantees that the minimum of $\mathcal{J}$ won't be on the boundary $\partial\mathcal{C}_{ad}$ (see also [24]).

Remark 2. If we assume that the admissible domain for control variables is $\mathcal{C}_{ad}^* = \{\boldsymbol{\sigma} = (\sigma_{il}, \sigma_{it}, \sigma_{el}, \sigma_{et}) \in (H^1(\Omega))^4 : \boldsymbol{\sigma}(x) \in [m, M]^4, \forall x \in \Omega\}$, we can actually prove the existence without using the Dunford-Pettis property. For the minimizing sequence $\boldsymbol{\sigma}^{(k)} \rightharpoonup \boldsymbol{\sigma}^*$ in $(L^2(\Omega))^4$, we also have $\nabla\boldsymbol{\sigma}^{(k)} \rightharpoonup \nabla\boldsymbol{\sigma}^*$ in $(L^2(\Omega;\mathbb{R}^d))^4$ by the uniform boundedness principle. Therefore $\{\boldsymbol{\sigma}^{(k)}\}$ is bounded in $(H^1(\Omega))^4$, which then implies a subsequence strongly convergent in $(L^2(\Omega))^4$. So with the admissible domain $\mathcal{C}_{ad}^*$ we may assume $\boldsymbol{\sigma}^{(k)} \to \boldsymbol{\sigma}^*$ pointwise a.e.

In the way of proving convergence (3.10), we obtain

$$\int_0^T \int_\Omega (\sigma_{il}^{(k)} - \sigma_{il}^*)\mathbf{a_l}^t\nabla(\phi\psi)\mathbf{a_l}^t\nabla u^{(k)} \leq ||(\sigma_{il}^{(k)} - \sigma_{il}^*)\mathbf{a_l}^t\nabla(\phi\psi)||_{L^2(Q)} \cdot ||\mathbf{a_l}^t\nabla u^{(k)}||_{L^2(Q)}$$

Notice that $\{||\mathbf{a_l}^t\nabla u^{(k)}||_{L^2(Q)}\}$ is uniformly bounded since $|\mathbf{a_l}| = 1$ and $\{\nabla u^{(k)}\}$ are bounded in $L^2(Q;\mathbb{R}^d)$. By the Dominated Convergence theorem,

$$||(\sigma_{il}^{(k)} - \sigma_{il}^*)\mathbf{a_l}^t\nabla(\phi\psi)||_{L^2(Q)} \to 0 \text{ as } k \to \infty.$$

4. Numerical solver. In this section, we briefly describe the space and time discretization techniques for solving the state and dual equations. For these preliminary 2D tests, we mainly focus on the reliability of the KKT approach for our

TABLE 4.1
Ionic model parameters

parameter	C_m	β	V_r	V_{th}	V_p	c_1	c_2	b	d
value	1	2000	-85	-75	15	0.26	0.1	0.013	0.8
unit	$\mu F cm^{-2}$	cm^{-1}	mV	mV	mV	ms^{-1}	ms^{-1}	ms^{-1}	-

optimization problem, so we don't pay much attention to the efficiency of the Bidomain solver. In our numerical simulation we use the finite element method(FEM) for the space discretization, and backward differentiation formula(BDF) method for the time discretization. In particular, the Rogers-McCulloch ionic model we consider here is given by

$$f(u,w) = \beta_1(u-V_r)(u-V_{th})(u-V_p) + c_2(u-V_r)w \tag{4.1}$$

$$g(u,w) = -\beta_2(u-V_r) + bdw \tag{4.2}$$

where $\beta_1 = \dfrac{c_1}{(V_p-V_r)^2}$, $\beta_2 = \dfrac{b}{V_p-V_r}$. The parameters used are from [25] and reported in Table 4.1. When comparing (4.1) with (3.1), we notice that in function (3.1) the potential u is actually a translation of the transmembrane potential by subtracting the rest potential V_r. With this setup, $g_{,u} = -\beta_2$, $g_{,w} = bd$ and $f_{,w} = c_2(u-V_r)$.

4.1. Space discretization. Let $V_h \subseteq V$ be the finite dimensional subspace of V containing piecewise linear basis functions with respect to spatial grids $\{x_j\}_{j=1}^N$, where N is the number of nodes. We denote $V_h = \text{span}\{\phi_j\}_{j=1}^N$. The Galerkin approximation of state equations takes the form: for each $t \in [0,T]$, find $(u_h, u_{e,h}) \in V_h \times V_h$, such that

$$\int_\Omega \frac{\partial u_h(t)}{\partial t} v_h + \int_\Omega \boldsymbol{\sigma}_i \nabla(u_h(t) + u_{e,h}(t)) \cdot \nabla v_h + \int_\Omega f(u_h(t), w(t)) v_h = \int_\Omega I_{si}(t) v_h, \quad \forall v_h \in V_h \tag{4.3}$$

$$\int_\Omega \boldsymbol{\sigma}_i \nabla u_h(t) \cdot \nabla v_h + \int_\Omega (\boldsymbol{\sigma}_i + \boldsymbol{\sigma}_e) \nabla u_{e,h}(t) \cdot \nabla v_h = \int_\Omega (I_{si}(t) - I_{se}(t)) v_h, \quad \forall v_h \in V_h \tag{4.4}$$

$$\frac{\partial w(t)}{\partial t} + g(u_h(t), w(t)) = 0 \tag{4.5}$$

The approximate finite element solution $(u_h, u_{e,h})$ has the form $u_h(x,y,t) = \sum_{j=1}^N u_j(t)\phi_j(x,y)$, $u_{e,h}(t) = \sum_{j=1}^N u_{e,j}(t)\phi_j(x,y)$. Denoting $\mathbf{u} = [u_j]$ and $\mathbf{u_e} = [u_{e,j}]$, the system (4.3-4.5) in matrix form would be

$$\mathbf{M}\frac{\partial \mathbf{u}}{\partial t} + \mathbf{S_i u} + \mathbf{S_i u_e} + \mathbf{f(u,w)} = \mathbf{I_{si}} \tag{4.6}$$

$$(\mathbf{S_i} + \mathbf{S_e})\mathbf{u_e} + \mathbf{S_i u} = \mathbf{I_{tr}} \tag{4.7}$$

$$\frac{\partial \mathbf{w}}{\partial t} + \mathbf{g}(\mathbf{u}, \mathbf{w}) = \mathbf{0} \tag{4.8}$$

where $\mathbf{S_i} = \{a_i(\phi_j, \phi_k)\}_{j,k=1}^N, \mathbf{S_e} = \{a_e(\phi_j, \phi_k)\}_{j,k=1}^N$ are the stiffness matrices, $\mathbf{M} = \{\int_\Omega \phi_j \phi_k\}_{j,k=1}^N$ is the mass matrix. The other vectors are $\mathbf{f}(\mathbf{u}, \mathbf{w}) = \{\int_\Omega f(\mathbf{u}, \mathbf{w})\phi_j\}_{j=1}^N$, $\mathbf{I_{si}} = \{\int_\Omega I_{si}\phi_j\}_{j=1}^N, \mathbf{I_{tr}} = \{\int_\Omega (I_{si} - I_{se})\phi_j\}_{j=1}^N, \mathbf{g}(\mathbf{u}, \mathbf{w}) = g(\mathbf{u}, \mathbf{w})$.

Similarly, we derive the matrix form of dual equations

$$\mathbf{M}\frac{\partial \mathbf{q}}{\partial t} - \mathbf{S_i p} - \mathbf{S_i q} - \mathbf{B}(\mathbf{v}, \mathbf{w})\mathbf{q} + \beta_2 \mathbf{M r} = -\mathbf{M_{obs}}(\mathbf{u} - \mathbf{u_{meas}}) \tag{4.9}$$

$$(\mathbf{S_i} + \mathbf{S_e})\mathbf{p} + \mathbf{S_i q} = \mathbf{0} \tag{4.10}$$

$$\frac{\partial \mathbf{r}}{\partial t} - bd\mathbf{r} - c_2(\mathbf{u} - V_r)^t \mathbf{q} = \mathbf{0} \tag{4.11}$$

where

$$\mathbf{M_{obs}} = \{\int_{\Omega_{obs}} \phi_j \phi_k\}_{j,k=1}^N,\ \mathbf{B}(\mathbf{v}, \mathbf{w}) = \{\int_\Omega f_{,u}\phi_j\phi_k\}_{j,k=1}^N,\ \mathbf{u_{meas}} = \{u_{meas}(x_j)\}_{j=1}^N.$$

Here x_j is the spatial node. When we do not have measurement on the nodes, we retrieve a measure from the available data by interpolation.

4.2. Time discretization. We denote Δt the time step and $t^i = i\Delta t$. For the time discretization, we use BDF2. The nonlinear term $f(u, w)$ in (4.6) is managed by a second order time extrapolation of u. We proceed similarly for the term u in (4.8) and the term q in (4.11). This means that for general smooth functions $h_1(u)$ and $h_2(q)$, we approximate the values as

$$h_1(u(t^{n+1})) = 2h_1(u(t^n)) - h_1(u(t^{n-1})) + O(\Delta t^2), \tag{4.12}$$

$$h_2(q(t^n)) = 2h_2(q(t^{n+1})) - h_2(q(t^{n+2})) + O(\Delta t^2). \tag{4.13}$$

In the forward solver for state equations, we use (4.12) with initial condition $u(t^{-1}) = u(t^0) = u_0$. In the backward solver for dual equations, we use (4.13) with initial condition $q(t^{K+1}) = q(t^K) = 0$, where $K = T/\Delta t$.

4.3. Algorithms. To solve the state and dual equations, we proceed as in Algorithm 1 described hereby. Then for finding the optimal set of parameters, we proceed as in Algorithm 2 illustrated in the sequel.

Algorithm 1 (Linear Solver)
Given initial value $\mathbf{u}(t^{-1}) = \mathbf{u}(t^0) = V_r,\ \mathbf{u_e}(t^{-1}) = \mathbf{u_e}(t^0) = 0,\ \mathbf{w}(t^{-1}) = \mathbf{w}(t^0) = 0$, for $i = 1$, up to $T/\Delta t$ do the following:

1. solve $\mathbf{w}(t^i)$ by

$$(\frac{3}{2\Delta t} + bd)\mathbf{w}(t^i) = \frac{2}{\Delta t}\mathbf{w}(t^{i-1}) - \frac{1}{2\Delta t}\mathbf{w}(t^{i-2}) + \beta_2(2\mathbf{u}(t^{i-1}) - \mathbf{u}(t^{i-2}) - V_r) \tag{4.14}$$

2. solve $\mathbf{u}(t^i)$ by

$$\begin{aligned}(\frac{3}{2\Delta t}\mathbf{M} + \mathbf{S_i})\mathbf{u}(t^i) = \frac{2}{\Delta t}\mathbf{M}\mathbf{u}(t^{i-1}) - \frac{1}{2\Delta t}\mathbf{M}\mathbf{u}(t^{i-2}) - \mathbf{S_i}(2\mathbf{u_e}(t^{i-1}) - \mathbf{u_e}(t^{i-2}))\\ - \mathbf{f}(2\mathbf{u}(t^{i-1}) - \mathbf{u}(t^{i-2}), \mathbf{w}(t^i)) + \mathbf{I_{si}}(t^i)\end{aligned} \tag{4.15}$$

3. solve $\mathbf{u_e}(t^i)$ by

$$(\mathbf{S_i}+\mathbf{S_e})\mathbf{u_e}(t^i) = -\mathbf{S_i}\mathbf{u}(t^i) + \mathbf{I_{tr}}(t^i) \tag{4.16}$$

Given the initial values $\mathbf{q}(t^{K+1}) = \mathbf{q}(t^K) = 0,\ \mathbf{p}(t^{K+1}) = \mathbf{p}(t^K) = 0,\ \mathbf{r}(t^{K+1}) = \mathbf{r}(t^K) = 0$, where $K = T/\Delta t$, for $i = K-1$, down to 0 do the following:

4. solve $\mathbf{r}(t^i)$ by

$$(\frac{3}{2\Delta t}+bd)\mathbf{r}(t^i) = \frac{2}{\Delta t}\mathbf{r}(t^{i+1}) - \frac{1}{2\Delta t}\mathbf{r}(t^{i+2}) - c_2(\mathbf{u}(t^i)-V_r)^t(2\mathbf{q}(t^{i+1})-2\mathbf{q}(t^{i+2})) \tag{4.17}$$

5. solve $\mathbf{q}(t^i)$ by

$$\begin{aligned}(\frac{3}{2\Delta t}\mathbf{M} + \mathbf{S_i} + \mathbf{B}(\mathbf{u}(t^i),\mathbf{w}(t^i)))\mathbf{q}(t^i) &= \frac{2}{\Delta t}\mathbf{M}\mathbf{q}(t^{i+1}) - \frac{1}{2\Delta t}\mathbf{M}\mathbf{q}(t^{i+2}) \\ - \mathbf{S_i}(2\mathbf{p}(t^{i+1}) - \mathbf{p}(t^{i+2})) + \beta_2\mathbf{M}\mathbf{r}(t^i) &+ \mathbf{M_{obs}}(\mathbf{u}(t^i) - \mathbf{u_{meas}}(t^i))\end{aligned} \tag{4.18}$$

6. solve $\mathbf{p}(t^i)$ by

$$(\mathbf{S_i}+\mathbf{S_e})\mathbf{p}(t^i) = -\mathbf{S_i}\mathbf{q}(t^i) \tag{4.19}$$

Algorithm 2 (Optimization)
Given initial guess $\boldsymbol{\sigma}^1$, for $k = 1$ up to the fulfillment of stopping criteria, do the following:

1. solve (u, u_e, w) from t^0 to t^K using $\boldsymbol{\sigma}^k$
2. compute cost function $\mathcal{J}(\boldsymbol{\sigma}^k)$
3. solve (q, p, r) from t^K to t^0 using $\boldsymbol{\sigma}^k$
4. compute the gradient of $\mathcal{J}$: $D\mathcal{J}(\boldsymbol{\sigma}^k)$
5. update $\boldsymbol{\sigma}^{k+1} = \boldsymbol{\sigma}^k + \gamma_k \boldsymbol{v}^k$

In step 5, we use the BFGS Quasi-Newton Optimization method for computing the search direction $\boldsymbol{v}^k$(we refer to [23] for details), and $\gamma_k \in (0, \infty)$ is computed through a cubic line search procedure. We use the BFGS algorithm implemented in the Freefem++ software [12]. The stopping criteria used is

$$||D\mathcal{J}(\boldsymbol{\sigma}^k)|| \leq \epsilon = 10^{-6}.$$

5. Numerical results. In this section we present a series of test cases inspired by the ones used in [9]. The computational domain is $\Omega = [0,1] \times [0,1] \in \mathbb{R}^2$ of size $1cm^2$. The sites for measurement were arranged into an array over the tissue domain, which consisted of 6×6 electrodes, with spacing of 1.667 mm. The site array points are shown in Figure 5.1.

The experimental mean conductivity values were taken as

$$\hat{\sigma}_{il} = 2.63mS/cm,\ \hat{\sigma}_{it} = 0.35mS/cm,\ \hat{\sigma}_{el} = 3.2mS/cm,\ \hat{\sigma}_{et} = 1.5mS/cm.$$

The fibre angle was chosen as $\theta = -48°$. In each test, four stimuli of $I_{si} = I_{se} = 100\mu Acm^{-2}$ were applied in the domain for a duration of $1ms$. Synthetic data was generated with the conductivity parameters

$$\sigma_{il} = 2.8mS/cm,\ \sigma_{it} = 0.26mS/cm,\ \sigma_{el} = 2.2mS/cm,\ \sigma_{et} = 1.3mS/cm.$$

We denote it by $\boldsymbol{\sigma}_{ref} = (2.8, 0.26, 2.2, 1.3)$.

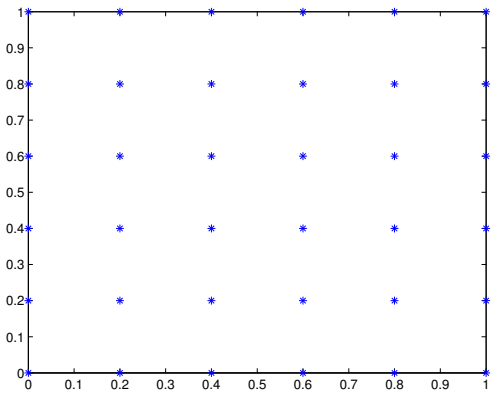

FIGURE 5.1. *Sites for measurement*

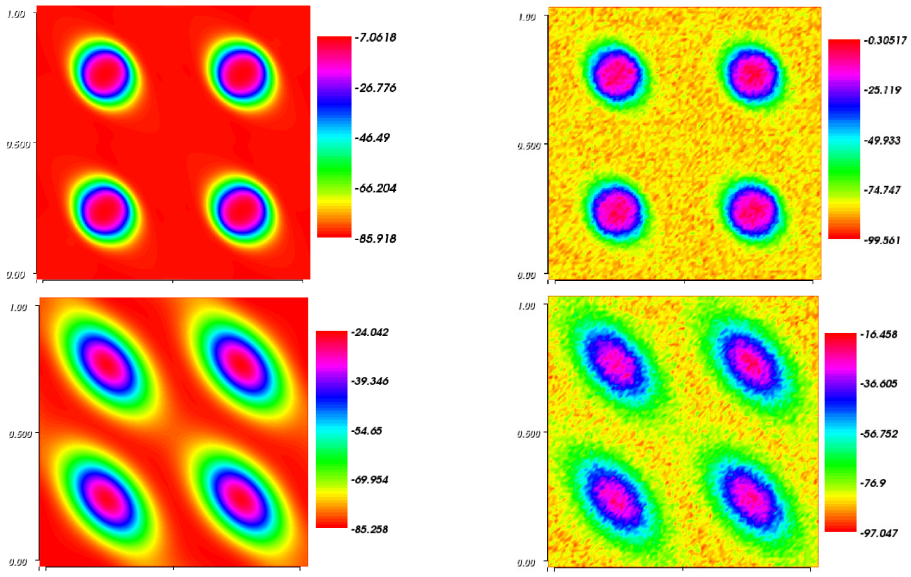

FIGURE 5.2. *Upperleft:* u_{meas} *at* $t = 2ms$. *Lowerleft:* u_{meas} *at* $t = 12ms$. *Upperright:* u_{meas} *at* $t = 2ms$ *with* 15% *noise. Lowerright:* u_{meas} *at* $t = 12ms$ *with* 15% *noise*

The noise added into the synthetic data was in a Gaussian normal distribution at each time step, with a zero mean, and its standard deviation was $(\sqrt{2}/2) \cdot 33p$, where p is the percentage of noise. 33 is used here to make a comparison with the Guassian noise in [9]. In Figure 5.2, left, the propagations of transmembrane potential on the tissue domain obtained with the forward solver are shown at $t = 2ms$ and $t = 12ms$. In Figure 5.2, right, the propagations with 15% noise added are shown.

Hereafter, we illustrate the results for several simulated experimental and numerical settings. The first test is a consistency check to outline the role of the noise in the global performance of the method. The subsequent tests illustrate the performances of the method on a data set synthetically generated by a numerical discretization

TABLE 5.1

The case generated data has the same mesh size as in optimization simulation. 51 nodes are on each boundary, $\alpha = 10^{-3}, T = 20ms$, and $\Delta t = 0.2ms$.

noise	10%	10%	10%	15%	15%	15%
dt_{snap}	0.2	0.6	1	0.2	0.6	1
σ_{il}	2.83208	2.81474	2.88077	2.8331	2.80349	2.98489
σ_{it}	0.258965	0.272091	0.246153	0.259489	0.283427	0.233413
σ_{el}	2.20867	2.24533	2.17742	2.22282	2.25126	2.1236
σ_{et}	1.25837	1.20986	1.22776	1.23981	1.15094	1.24476
# fwd	15	21	19	19	22	22
# bwd	15	15	15	16	15	17

TABLE 5.2

The case generated data has much finer mesh size than optimization simulation. 51 nodes are on each boundary, $\alpha = 10^{-5}, T = 25ms, \Delta t = 0.025ms$, and $dt_{snap} = 0.5ms$.

noise	0%	10%	15%
$\sigma_{il}\|e_{il}$	2.7504|0.0496	2.72529|0.07471	2.71204|0.08796
$\sigma_{it}\|e_{it}$	0.208004|0.051996	0.210232|0.049768	0.211344|0.048656
$\sigma_{el}\|e_{el}$	2.22046|0.02046	2.23888|0.03888	2.24965|0.04965
$\sigma_{et}\|e_{et}$	1.31297|0.01297	1.32505|0.02505	1.33751|0.03751
Initial $\mathcal{J}$	0.442516	0.45743	0.47792
Final $\mathcal{J}$	0.00161641	0.0187802	0.0403941
Iter. fwd|bwd	18|16	21|18	19|18

different than the one used for solving the inverse problem.

Test 1: The discretization method for generating data is the same as the one for solving (u, u_e, w) during optimization process, that is FEM P1 with 51 nodes on each boundary for space discretization, and BDF2 with $\Delta t = 0.2ms$ for time discretization. Simulation with each searched value $\boldsymbol{\sigma}$ was run for $T = 20ms$. We report the result in Table 5.1, in which dt_{snap} denotes the time step for measurement. The initial guess is $\boldsymbol{\sigma} = (1, 1, 1, 1)$. The Tikhonov coefficient is $\alpha = 10^{-3}$. As we see in the table, even with 15% noisy data and big snapshot time step dt_{snap}, we can still get optimized result quite close to $\boldsymbol{\sigma}_{ref}$. This result is comparable with the result in [9] Table 3, since we need at most 39 bidomain solvers vs about 100 required in [9]. (Notice that the backward solver has the same complexity as the forward solver.)

Test 2: In this test the space discretization method for generating data is FEM P2 with 251 nodes on each boundary, and the time step is $\Delta t = 0.0025ms$.. For simulation during optimization procedure, we use FEM P1 with 51 nodes on each boundary and $\Delta t = 0.025ms$. The result is shown in Table 5.2. Quantities e refer to the corresponding error $|\sigma^{estimated} - \sigma^{exact}|$. In this test, $T = 25ms, \alpha = 10^{-5}$, and dt_{snap} is always $0.5ms$. We can see, wih 15% noisy data, we get a final estimate featuring an error (0.08796, 0.048656, 0.04965, 0.03751) and a relative error (3.1%, 18.7%, 2.3%, 2.9%). Although the error e_{it} is pretty high, the results are expected since the solution of the Bidomain equation is more sensitive to the longitudinal rather than to the tangential conductivities.. The solution process requires 37 Bidomain solutions, which is a significant reduction in comparison with results of [9]. Yet, the

TABLE 5.3

The case generated data has much finer mesh size than optimization simulation. 101 nodes are on each boundary, $\alpha = 10^{-5}, T = 25ms, \Delta t = 0.025ms,$ *and* $dt_{snap} = 0.5ms$.

noise	0%	10%	15%
$\sigma_{il}\|e_{il}$	2.91352|0.11352	2.88935|0.08935	2.93269|0.13269
$\sigma_{it}\|e_{it}$	0.248622|0.011378	0.273256|0.013256	0.260421|0.000421
$\sigma_{el}\|e_{el}$	2.14708|0.05292	2.26143|0.06143	2.14895|0.05105
$\sigma_{et}\|e_{et}$	0.953514|0.346486	0.762194|0.537806	0.967035|0.332965
Initial $\mathcal{J}$	0.109463	0.111839	0.116154
Final $\mathcal{J}$	0.000809365	0.00516467	0.0102197
Iter. fwd|bwd	28|22	35|24	46|28

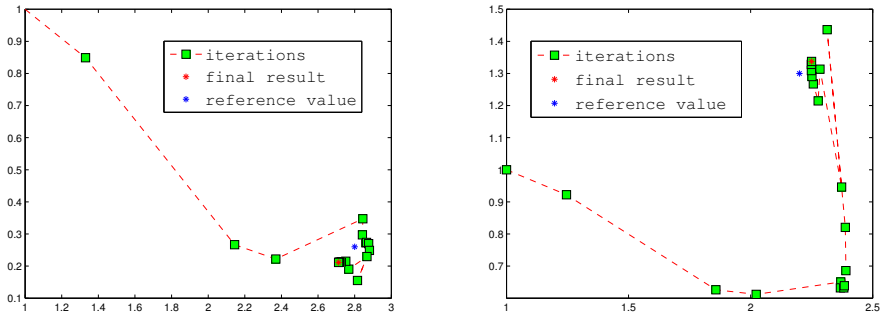

FIGURE 5.3. *Left: Iterations for* $(\sigma_{il}, \sigma_{it})$*; Right: Iterations for* $(\sigma_{el}, \sigma_{et})$

improvement of the computational costs is one of the important follow-ups of the present work (see Section 6).

Test 3: Compared with test 2, we use 101 nodes on each boundary for space discretization during optimization. We report the result in Table 5.3. With 15% noisy data, we get final results with error (0.13269, 0.000421, 0.05105, 0.332965) and a relative error (4.7%, 0.2%, 2.3%, 25.6%). Here with finer mesh on the computational domain we get slightly worse results. We speculate that this is because the errors induced by the poor sampling and the noise is dominating the error of the numerical solution of the Bidomain equations. Improvements in the estimate can be achieved with more data.

To have a better insight on the efficiency of our optimization method, we plot the searched value at each optimization iteration in Figure 5.3. The value found at each iteration is denoted by a (green) box, connected by dashed (red) lines. We draw $(\sigma_{il}, \sigma_{it})$ in Figure 5.3 left and $(\sigma_{el}, \sigma_{et})$ in Figure 5.3 right. This figure corresponds to Test 2 with 15% noisy data. The exact reference value is denoted by an asterisk. We see that after about 15 iterations the searched values are close to the exact values.

Finally, to have a better understanding on the reliability of our estimates, we run the forward simulation using both the reference value $\boldsymbol{\sigma}_{ref}$ and the estimated value obtained from Test 3 with 15% noisy data. In Figure 5.4, we show the propagation of the action potential at the tissue center. In spite of the presence of noise, we notice that the potential propagation is well captured by the Bidomain equation with the estimated conductivities found by the optimization procedure. In other terms, the

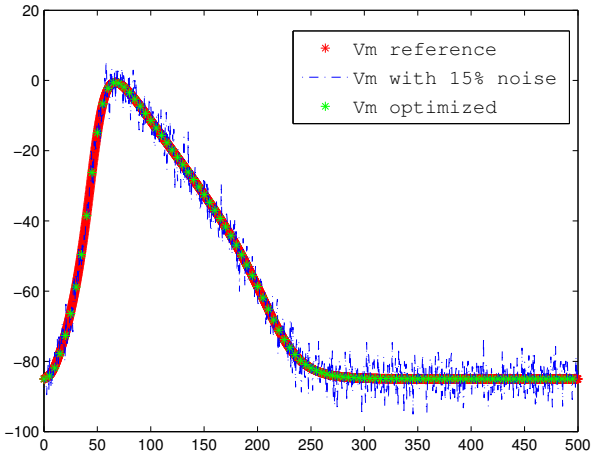

FIGURE 5.4. *Action potential in the tissue center*

error on the estimated conductivities does not prevent the correct capturing of the potential propagation in the numerical solution of the Bidomain equations.

6. Conclusions and developments. The accurate quantification of cardiac conductivities is crucial for extending computational electrocardiology from medical research to clinical practice. With this motivation, we have investigated a variational data assimilation approach for providing conductivity estimates from potential measurements. Other approaches are possible, like the one based on Kalman filtering techniques (see e.g. [21]). We proved the correct statement of the problem, by showing the existence of a set of parameters minimizing the (regularized) mismatch between numerical results and measurements. Here we have limited to 2D problems for the sake of simplicity. The next steps of the present work will be to extend the results to 3D cases and to perform validation with *in vitro* experiments. We do expect to face formidable computational costs then, since the iterated solution of the Bidomain system and its dual in real geometries may be fairly demanding [8, 20]. For this reason, we will investigate possible model reduction techniques, to replace in the optimization process with low-dimensional models, as done, for instance, in [2] for the estimation of compliance in arteries.

Another important direction we intend to work is the rigorous quantification of uncertainty induced by the presence of noise. In this case, the conductivities estimated will be defined by a probability density function whose moments depend on the noise and the Bidomain problem (see e.g. for fluid dynamics [33]).

REFERENCES

[1] R.A. Adams and J.J.F. Fournier. *Sobolev Spaces*. Elsevier, Second edition 2003.
[2] L. Bertagna, A. Veneziani, A model redution approach to the variational estimation of arterial compliance, in preparation (2013).
[3] Y. Bourgault, Y. Coudière, and C. Pierre. Existence and uniqueness of the solution for the bidomain model used in cardiac electrophysiology. *Nonlinear analysis: Real world applications*, 10(1):458–482, 2009.
[4] R.H. Clayton, O. Bernus, E.M. Cherry, H. Dierckx, F.H. Fenton, L. Mirabella, A.V. Pan-

filov, F.B. Sachse, G. Seemann, and H. Zhang. Models of cardiac tissue electrophysiology: Progress, challenges and open questions. *Progress in Biophysics and Molecular Biology*, 104(1-3):22–48, 2011.

[5] L. Clerc. Directional differences of impulse spread in trabecular muscle from mammalian heart. *J Phisiology*, 255:335–346, 1976.

[6] M. D'Elia, L. Mirabella, T. Passerini, M. Perego, M. Piccinelli, C. Vergara, and A. Veneziani. *Applications of variational data assimilation in computational hemodynamics*, chapter 12, pages 363–394. MS & A. Springer, 2011.

[7] Geselowitz, D. B. An application of electrocardiographic lead theory to impedance plethysmography. *IEEE Trans. Biomed. Eng.* BME-18:38-41, 1971.

[8] L. Gerardo Giorda, L. Mirabella, F. Nobile, M. Perego, and A. Veneziani. A model-based block-triangular preconditioner for the bidomain system in electrocardiology. *Journal of Computational Physics*, 228(10):3625–3639, 2009.

[9] L. S. Graham and D. Kilpatrick. Estimation of the bidomain conductivity parameters of cardiac tissue from extracellular potential distributions initiated by point stimulation. *Annals of Biomedical Engineering*, 38(12):3630–3648, 2010.

[10] L.S. Graham, D. Kilpatrick, F. Sainsbury, and A.C. Young. The determination of the bidomain conductivity values of heart tissue. *Computers in Cardiology*, 35:193–196, 2008.

[11] M.D. Gunzburger. *Perspectives in Flow Control and Optimization*, SIAM, 2003.

[12] F. Hecht. Freefem++ software. *http://www.freefem.org/ff++*, 2013.

[13] P.R. Johnston. A sensitivity study of conductivity values in the passive bidomain equation. *Mathematical biosciences*, 232(2):142–150, 2011.

[14] B.J. Kogan. *Introduction to computational cardiology*. Springer-Verlag New York Inc, 2009.

[15] K. Kunisch and M. Wagner. Optimal control of the bidomain system (i): The monodomain approximation with the rogers-mcculloch model. Technical Report Preprint 03, Institute of Mathematics, 2011.

[16] K. Kunisch and M. Wagner. Optimal control of the bidomain system (ii): Uniqueness and regularity theorems for weak solutions. Technical Report SFB-Report 08, Institute for Mathematics and Scientific Computing, 2011.

[17] K. Kunisch and M. Wagner. Optimal control of the bidomain system (iii): Existence of minimizers and first-order optimality conditions. Technical Report SFB-Report 31, Institute for Mathematics and Scientific Computing, 2011.

[18] P. LeGuyader, F. Trelles, and P. Savard. Extracellular measurement of anisotropic bidomain myocardial conductivities. i. theoretical analysis. *Annals Biomed Eng*, 29:862–877, 2001.

[19] P. Lin. *Köthe-Bochner Function Spaces*. Birkhäuser, 2003.

[20] L. Mirabella, F. Nobile, and A. Veneziani. An *a posteriori* error estimator for model adaptivity in electrocardiology. *Computer Methods in Applied Mechanics and Engineering*, 200(37):2727–2737, 2011.

[21] P. Moireau and D. Chapelle. Reduced-order unscented kalman filtering with application to parameter identification in large-dimensional systems. *ESAIM: Control, Optimisation and Calculus of Variations*, 17:380–405, 2011.

[22] C. Nagaiah, K. Kunisch, and G. Plank. Numerical solution for optimal control of the reaction-diffusion equations in cardiac electrophysiology. *Computational Optimization and Applications*, 49(1):149–178, 2011.

[23] J. Nocedal and S.J. Wright. *Numerical optimization*. Springer, Second edition, 2006.

[24] Mauro Perego, Alessandro Veneziani, and Christian Vergara. A variational approach for estimating the compliance of the cardiovascular tissue: An inverse fluid-structure interaction problem. *SIAM J. Scientific Computing*, 33(3):1181–1211, 2011.

[25] A.J. Pullan, L.K. Cheng, and M.L. Buist. *Mathematically Modelling the Electrical Activity of the Heart: From Cell to Body surface and back again*. World Scientific Pub Co Inc, 2005.

[26] D.E. Roberts, L.T. Hersh, and A.M. Scher. Influence of cardiac fiber orientation on wavefront voltage, conduction, velocity and tissue resistivity in the dog. *Circ Res*, 44(5):701–712, 1979.

[27] D.E. Roberts and A.M. Scher. Effect of tissue anisotropy on extracellular potential fields in canine myocardium in situ. *Circ Res*, 50(3):342–351, 1982.

[28] F.B. Sachse. *Computational cardiology: modeling of anatomy, electrophysiology, and mechanics*, volume 2966. Springer Verlag, 2004.

[29] R. Sadleir and C. Henriquez. Estimation of cardiac bidomain parameters from extracellular measurement: two dimensional study. *Annals of biomedical engineering*, 34(8):1289–1303, 2006.

[30] J.G. Stinstra, B. Hopenfeld, and R.S. MacLeod. A model for the passive cardiac conductivity. *International Journal of Bioelectromagnetism*, 5(1):185–186, 2003.

[31] J.G. Stinstra, B. Hopenfeld, and R.S. MacLeod. On the passive cardiac conductivity. *Annals of biomedical engineering*, 33(12):1743–1751, 2005.

[32] A. Veneziani, C. Vergara, Inverse problems in Cardiovascular Mathematics: towards patient-specific assimilation and optimization, editorial to appear in Int J Num Meth Biomed Eng (2013)

[33] Alessandro Veneziani and Marta D'Elia. Uncertainty quantification for data assimilation in a steady incompressible Navier-Stokes problem. *ESAIM: Mathematical Modelling and Numerical Analysis*, doi:10.1051/m2an/2012056, to appear 2013